Wave Motion 104 (2021) 102750

Contents lists available at ScienceDirect

Wave Motion

journal homepage: www.elsevier.com/locate/wamot

Low-frequency flexural wave attenuation in metamaterial sandwich beam with hourglass lattice truss core

Zhenkun Guo [a,b,c], Guobiao Hu [b], Vladislav Sorokin [b,*], Lihua Tang [b,*], Xiaodong Yang [c], Jun Zhang [a]

[a] Beijing Key Laboratory of Performance Guarantee on Urban Rail Transit Vehicles, Beijing University of Civil Engineering and Architecture, Beijing, 102616, China
[b] Department of Mechanical Engineering, University of Auckland, Auckland 1010, New Zealand
[c] College of Mechanical Engineering, Beijing University of Technology, Beijing 100022, China

ARTICLE INFO

Article history:
Received 9 June 2020
Received in revised form 9 December 2020
Accepted 20 April 2021
Available online 1 May 2021

Keywords:
Metamaterial sandwich beam
Metamaterial dual-beam
Hourglass lattice core
Band gap
Local resonance
Transfer matrix method

ABSTRACT

Though lightweight sandwich structures have been extensively applied in practical engineering, it remains a challenge to control wave propagation and vibration in these structures in a low-frequency range. In this work, the band structure of flexural waves in a metamaterial sandwich beam (MSB) with hourglass lattice truss core is investigated using the transfer matrix method (TMM). The hourglass truss structure with lumped masses is modelled as a series of local resonators with determined equivalent stiffnesses and masses. A metamaterial dual-beam (MDB) model is then established to describe the MSB, and the MDB model is noted to be equivalent to the conventional metamaterial beam (CMB) model under base excitation. The MSB is further studied directly by the finite element method that confirmed the MSB can be represented by the CMB through the transmittance analysis and band structure analysis. Subsequently, parametric study is performed to investigate the effects of the material and structural parameters on the band structures of the MSB. This work provides a roadmap of modelling of lightweight lattice sandwich beams with complex core structures and presents guidelines for applying sandwich beams to control wave propagation.

1. Introduction

Metamaterials are artificial periodic structures that can generate band gaps that are frequency ranges within which the propagation of waves is forbidden [1–7]. Because of this intriguing phenomenon, extensive research interests have been attracted into exploring the theory and applications of metamaterials in wave attenuation and vibration control. There exist two basic band gap generation mechanism, i.e., Bragg scattering (BS) [8–10] and local resonance (LR) [11,12]. BS exists in phononic crystal and the band gap occurs in the frequency range where wavelengths are of the same order of magnitude as the lattice constant. Thus, a large lattice constant is required to attenuate low-frequency waves, which is often not realistic in the design of practical engineering structures. Different from phononic crystals, based on the local resonance mechanism, metamaterials could easily generate a low-frequency band gap. Therefore, enormous efforts have been devoted to studying and tailoring band gaps of metamaterials.

* Corresponding authors.
E-mail addresses: v.sorokin@auckland.ac.nz (V. Sorokin), l.tang@auckland.ac.nz (L. Tang).

https://doi.org/10.1016/j.wavemoti.2021.102750
0165-2125/

As well-known that lots of engineering structures, such as bridges [13], spacecraft arms [14] and building frames [15] can often be modelled as flexible beams, if the transverse dimension is much smaller than the longitudinal dimension. The terminology 'beam' implies that the structure is relatively thin and the transverse modes occur at lower frequencies than longitudinal modes. For this reason, in the low-frequency domain, the transverse vibration of a beam-like structure has a more significant effect on the structural safety and stability. Hence, significant attention has been given to study the transverse vibration of beams [16–18]. In recent years, some researchers focused on using metamaterials for low-frequency flexural wave attenuation of continuous systems. By using the transfer matrix method (TMM), Yu et al. [11,19] researched the flexural wave attenuation of LR beams, in which the local resonators were made up of soft rubber rings and copper rings. Xiao et al. [20] investigated the band gap formation mechanism with an analytical method on basis of the periodic structure theory and spectral element method. In order to broaden the width of the band gap, periodic local resonators arrays with different resonant frequencies were designed and studied [21,22]. Another way to achieve a wide band gap is to construct a resonator with multiple degrees of freedom (DOF). Pai et al. [23,24] proposed a two-DOF subsystem to be attached to the beam and plate for inducing two band gaps. The inertial force produced by the resonance of the absorber enhances the wave attenuation. Wang et al. [25,26] theoretically and numerically studied flexural vibration of a metamaterial beam and plate with attached lateral local resonators. They found it could generate two band gaps to attenuate the flexural vibration, for which the formation mechanism is due to the transition from the flexural wave to longitudinal wave by a four-link-mechanism, which stimulates the lateral resonance to generate inertial force to counterbalance the shear force of the plate. Miranda Jr. et al. [27] studied flexural waves propagation in a metamaterial plate using Kirchhoff–Love theory, and found that by changing the arrays of multiple DOF resonators, the locally resonant band gaps could be effectively widened. By combining auxeticity and phononic crystals band gap properties, D'Alessandro et al. [28] obtained a tunable wide band gap in numerical and analytical models. On the other hand, some researchers installed piezoelectric shunts periodically on host structures as adjustable resonators to control vibration and wave propagation [29–31].

In addition to widening the band gaps, many researchers poured attention into achieving band gaps in low or ultra-low-frequency range. Since the band gap location of LR metamaterial beam mainly depends on the natural frequency of resonators, to achieve low-frequency band gap, one has to increase the mass or decrease the stiffness of the resonators. The concept of inertial amplification is proposed by Yilmaz et al. [32] to embed the amplification mechanism into the unit cell, which could effectively increase the inertia of resonators and reduce the resonance frequency. Assouar et al. [33] presented hybrid metamaterial plates that consisted of periodic stepped pillars and holes, in which the waves scattered simultaneously by the pillars and holes in certain frequency ranges generate wide and low band gaps. Zhou et al. [34] presented a novel resonator which combines a vertical spring with two oblique springs that provide negative stiffness in vertical direction, and found the band gap could be shifted into very low frequencies by tuning the stiffness of the oblique springs. D'Alessandro et al. [35] presented a novel 3D elastic periodic structure with a distributed set of local resonators to realize low-frequency band gaps. Fang et al. [36] unveiled the nonlinear chaotic mechanism in nonlinear acoustic metamaterials (NAMs) for achieving band gaps and chaotic bands in an ultra-low and ultra-broad frequency range.

In past decades, many researchers focused on the dynamics of sandwich structures [37–41], because sandwich structures with high strength and low weight are ideal solutions to realize lightweight characteristics in practical applications for bearing large bending load. In order to reduce the possibility of catastrophic accidents caused by vibration, it is necessary to control the vibration levels of the sandwich structures. Relative to the traditional active [42] and passive [43] vibration control methods, as well as Bragg scattering metamaterial [44], the metamaterial theory could generate and tune band gaps to attenuate the flexural wave in specific low-frequency ranges. Chen et al. [45,46] investigated flexural vibration behaviour of a sandwich beam with local resonators embedded into foam cores analytically and experimentally. It is assumed that resonators were uniformly distributed along the sandwich beam with the volume averaging technique. Their proposed model, however, did not account for the effect of the periodicity of discrete resonators on band structures of the sandwich system. Based on this work, Sharma and Sun [47] used the phased array method to calculate propagation constants of a sandwich beam with resonators inserted into the core layer, concluding a more clear explanation for the effect of periodicity of resonators on flexural vibration of the sandwich beam. Furthermore, Chen and Huang [48] proposed a sandwich structure embedded with multiple resonators that can generate a plurality of band gaps with excellent wave attenuation characteristics. Nevertheless, widths of band gaps for the proposed single resonator or multiple resonators sandwich structures are still relatively narrow, which cannot completely satisfy the requirement of practical applications such as the blast- or impact-induced wave in which the frequency ranges tend to be quite broad. For this reason, Chen et al. [49] added the dissipative multiple resonators to the core layer of sandwich beams to achieve a wide wave absorption band efficiently.

Though some literature has been published on wave attenuation of sandwich structures, most of them inserted lumped mass–spring resonators into the idealized homogenized core [45–49]. Thus, the proposed systems are not realistic especially in terms of the implementation of the resonators. Other researchers proposed some practical meta-structures designed with complicated micro-structures and manufactured using 3D printing technology [7,35]. However, the proposed structures are relatively arbitrary. Though excellent dynamic properties are achieved in the proposed structures, the static properties which are also of great importance in the engineering field [50–52] can not be guaranteed. For this reason, based on the sandwich beam with hourglass truss structure whose static properties have already been

experimentally studied and proved to outperform those with traditional lattice cores [53–55], such as the hourglass truss structure with relative density ranging from about 1.1% to 2.7% has 40%–60% higher shear strength and 26%–47% higher out-of-plane compressive strength than those of the pyramidal truss structure with similar relative density, as well as better bending strength. This paper proposes a novel metamaterial sandwich structure to realize wave attenuation in a low-frequency range. The hourglass truss structure is made up of eight struts. It is similar to a two-layer pyramidal truss structure but has a smaller slenderness ratio and a superior resistance to the buckling of the core layer. The oblique struts in the hourglass core sandwich beam are readily used as the springs for implementing the local resonators, making the proposed meta-structure relatively more realistic. Besides of the novel structure, from the methodology perspective, the model presented in this work simplifies the oblique struts as vertical springs to help reduce the difficulty in mathematical modelling.

Researchers have investigated the dynamic behaviour of such structures [56,57], however, designing the hourglass core sandwich beam with a metamaterial characteristic for vibration suppression has never been found in the existing literature. In this work, we develop a novel approach to establish the model of the metamaterial sandwich beam with hourglass core and investigate its band gap phenomenon. A lumped mass is added on the intersection of the eight oblique struts for the hourglass structure unit cell to assemble a resonator, in which the oblique struts provide elastic stiffness in vertical direction. The equivalent stiffness of the hourglass truss structure is obtained by using Hook's law. The metamaterial sandwich beam (MSB) is then simplified into a metamaterial dual-beam (MDB), which can eventually be modelled as a conventional metamaterial beam (CMB) under base excitation. The feasibility of using the simplified CMB model to represent MSB is validated based on both transmittance and band structure analysis for the MSB using finite element method (FEM). The effects of material and structural parameters on the band structures of MSB are then studied.

2. Theoretical modelling

The relatively complicated lattice core structure imposes a great difficulty on the modelling of the metamaterial sandwich beam (MSB). This research aims to propose an easily implementable modelling approach to address this issue by interpreting the hourglass lattice core structure as an equivalent mass–spring system. In the field of composite structures and materials, it is often assumed that the lattice core has negligible influence on the bending stiffness and only contributes to the shear stiffness of the sandwich beam [42]. It is thus reasonable to assume that at the conjunction between the truss core and the face sheets only the transverse force interaction is present. Therefore, we propose to regard the truss structure as a series of local resonators which also only has the transverse force interaction with the host beam. In this section, the equivalent stiffness of the resonators is derived. Subsequently, a metamaterial dual-beam (MDB) model is established to describe the MSB. Under base excitation, the MDB model is then noted to be equivalent to the conventional metamaterial beam (CMB) model. The MSB with complicated truss core structure is finally modelled as the CMB with derived equivalent parameters.

2.1. Equivalent stiffness of the hourglass truss structure

In this section, the equivalent stiffness of the hourglass truss structure is derived basing on Hook's law. Fig. 1 shows the hourglass lattice truss structure that consists of eight identical oblique struts with radius and length of r_c and l, respectively, as well as a lumped mass m. The height of the hourglass lattice structure , i.e., the distance between the two face sheets, is h_c. The inclination angle of the truss denoted by α and the span of one hourglass unit cell (i.e., lattice constant) denoted by a are related by $a = h_c/\tan\alpha$. The Young's modulus and mass density of the mother material are E and ρ, respectively. A lumped mass denoted by m is added on the intersection of the eight symmetrical oblique struts. Due to symmetry of the structure, only four struts in one plane are depicted in Fig. 2(a). It is noted the equivalent stiffness k' of the two struts presented in Fig. 2(a) is only quarter of that of the whole hourglass truss core structure. Fig. 2(b) shows the equivalent lumped parameter representation of the four strut structure. The equivalent stiffness of the whole hourglass core structure with eight struts should be $4k'$.

As shown in Fig. 2(a), the planar four strut structure intersects at point H and the four struts are all inclined at the same angle of α with respect to the horizontal. With a vertical concentrated force F applied at H, the intersection point moves to H'. Considering the force balance in x- and y-directions, one obtains

$$\begin{aligned} &F_{HC}\cdot\cos\alpha - F_{HB}\cdot\cos\alpha + F_{HD}\cdot\cos\alpha - F_{HE}\cdot\cos\alpha = 0 \\ &F_{HB}\cdot\sin\alpha + F_{HC}\cdot\sin\alpha + F_{HD}\cdot\sin\alpha + F_{HE}\cdot\sin\alpha = F \end{aligned} \tag{1}$$

where F_{HB}, F_{HC}, F_{HD}, F_{HE} are the axial forces of the four struts, respectively. Due to the symmetry of the four struts, the axial forces in the four struts are supposed to be the same and can be derived from Eq. (1)

$$F_{HB} = F_{HC} = F_{HD} = F_{HE} = \frac{F}{4\sin\alpha} \tag{2}$$

Under the small deformation assumption, the axial deformation of the four struts (i.e., Δl_{HB}, Δl_{HC}, Δl_{HD}, Δl_{HE}) can be approximated as

$$\Delta l_{HB} = \Delta l_{HC} = \Delta l_{HD} = \Delta l_{HE} \approx -l_{HH'}\sin\alpha' \approx -l_{HH'}\sin\alpha \tag{3}$$

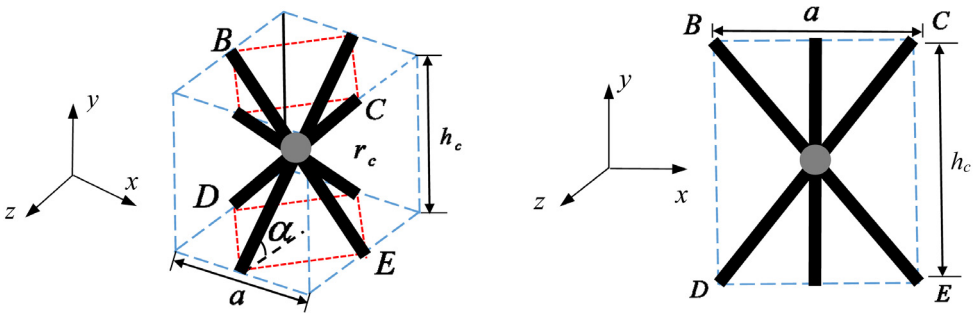

Fig. 1. (a) Hourglass lattice truss structure. (b) Front view of the hourglass lattice truss structure.

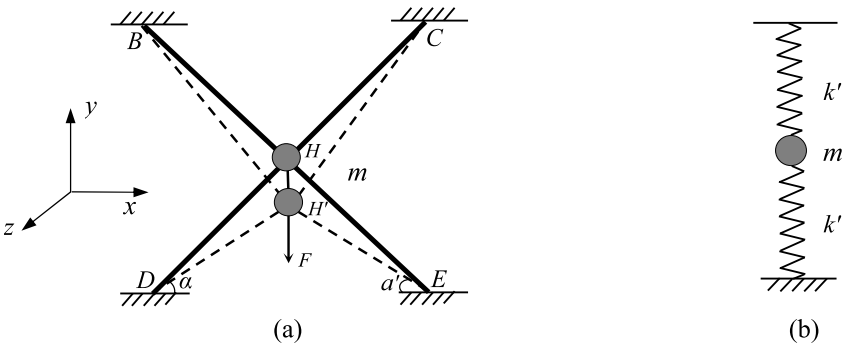

Fig. 2. (a) Deformation diagram of the clamped oblique struts under a concentrated force, (b) equivalent resonator.

where $l_{HH'}$ represents the displacement of point H in the vertical direction, and α' represents the inclination angle of the struts after deformation. Within the elastic deformation regime, the relation between the axial deformation and the force can be expressed as

$$\Delta l_{HB} = \frac{F_{HB} l_{HB}}{E_s A_s} \tag{4}$$

where l_{HB} denotes the length of the struts, E_s and A_s are the Young's modulus and cross-sectional area, respectively. By substituting Eqs. (2) and (3) into Eq. (4), the relation between the vertical deformation and the applied force on the truss structure can be obtained

$$l_{HH'} = \frac{F l_{HB}}{4 E_s A_s \sin 2\alpha} \tag{5}$$

By representing the four struts system as two springs connected in series, the equivalent stiffness of each spring can be derived by the Hook's law

$$k' = \frac{F}{2 l_{HH'}} = \frac{2 E_s A_s \sin 2\alpha}{l_{HB}} \tag{6}$$

Noting that since the actual hourglass truss structure (Fig. 1) consists of two identical four struts systems (Fig. 2(a)) in two orthogonal planes [53], by representing the whole hourglass core structure as two springs connected in series, the equivalent stiffness of the springs should be

$$k = 2k' = \frac{4 E_s A_s \sin 2\alpha}{l_{HB}} \tag{7}$$

2.2. Equivalent MDB model

By modelling the truss structure as a spring system, the metamaterial sandwich beam (MSB) as shown in Fig. 3 can be represented as a metamaterial dual-beam (MDB) system attached with local resonators in the periodic manner as shown in Fig. 4(a). Furthermore, the MDB is approximated as conventional metamaterial beam (CMB) in theoretical modelling as shown in Fig. 4, and it is worth mentioning that the stiffness of spring and thickness of beam in Fig. 4(b) is equal to the sum of two springs and beams in Fig. 4(a), respectively. The top and bottom face sheets have the same geometrical

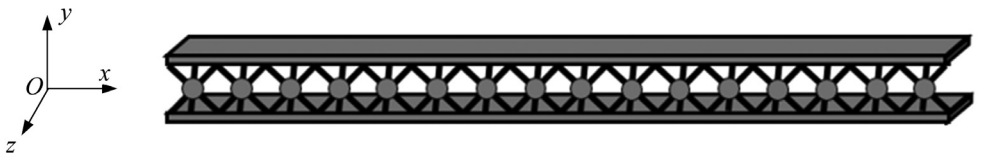

Fig. 3. Schematic of metamaterial sandwich beam (MSB) with hourglass lattice truss core.

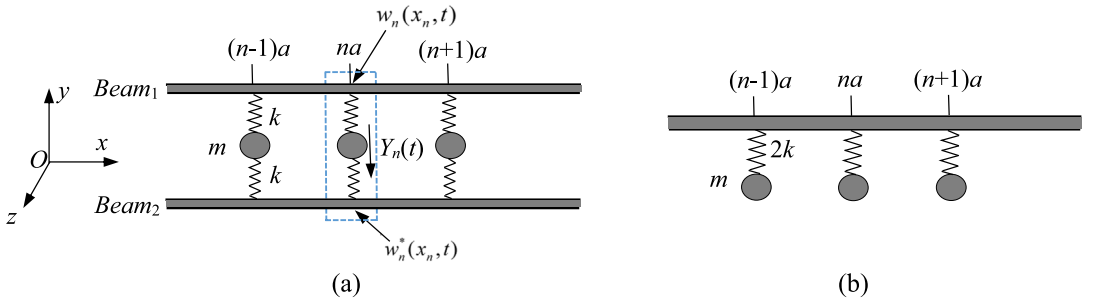

Fig. 4. Model of (a) MDB, (b) CMB.

dimensions and denoted as $Beam_1$ and $Beam_2$, respectively. Based on the Euler–Bernoulli beam theory, the governing equations for the free flexural vibration of the two beams can be written as follows:

$$EI\frac{\partial^4 w}{\partial x^4}+\rho A\frac{\partial^2 w}{\partial t^2}=0,\ EI\frac{\partial^4 w*}{\partial x^4}+\rho A\frac{\partial^2 w*}{\partial t^2}=0 \tag{8}$$

where w and w^* denote the deflection of $Beam_1$ and $Beam_2$ shown in Fig. 4(a), respectively. A is the cross-sectional area of the beams and I is the inertia moment with respect to the axis that perpendicular to x-axis. By focusing on the steady-state harmonic response, one can assume $w(x,t)=W(x)e^{j\omega t}$, $w*(x,t)=W*(x)e^{j\omega t}$, where ω is the circular frequency. Considering the n-th cell of the MDB as shown in the dashed box in Fig. 4(a), the displacement amplitudes of $Beam_1$ and $Beam_2$ are written as

$$\begin{aligned}&W_n(x)=A_n\cos(\beta x)+B_n\sin(\beta x)+C_n\cosh(\beta x)+D_n\sinh(\beta x)\\&W_n^*(x)=A_n^*\cos(\beta x)+B_n^*\sin(\beta x)+C_n^*\cosh(\beta x)+D_n^*\sinh(\beta x)\end{aligned} \tag{9}$$

where $\beta^4=\rho A\omega^2/EI$. The equation of motion of the n-th local resonator is

$$k[w_n(x_n,t)-y_n(t)]+k[w_n^*(x_n,t)-y_n(t)]=m\ddot{y}_n(t) \tag{10}$$

where $y_n(t)=Y_n e^{j\omega t}$ is displacement of the resonator and Y_n is the amplitude. The continuities of displacement, slope, bending moment and shear force at the interface between (n-1)-th cell and nth cell require

$$\begin{cases}W_n(0)=W_{n-1}(a)\\W_n'(0)=W_{n-1}'(a)\\EIW_n''(0)=EIW_{n-1}''(a)\\EIW_n'''(0)+F_n=EIW_{n-1}'''(a)\\W_n^*(0)=W_{n-1}^*(a)\\W_n^{*'}(0)=W_{n-1}^{*'}(a)\\EIW_n^{*''}(0)=EIW_{n-1}^{*''}(a)\\EIW_n^{*'''}(0)+F_n=EIW_{n-1}^{*'''}(a)\end{cases} \tag{11}$$

where $F_n=\frac{mk\omega^2}{m\omega^2-2k}[W_n(0)+W_n^*(0)]$. The transfer matrix of the coefficients vector can be obtained

$$\begin{aligned}&\boldsymbol{\psi}_n=[A_n,B_n,C_n,D_n,A_n^*,B_n^*,C_n^*,D_n^*]^T\\&\boldsymbol{\psi}_n=\mathbf{T}\boldsymbol{\psi}_{n-1}=\mathbf{K}^{-1}\mathbf{H}\boldsymbol{\psi}_{n-1}\end{aligned} \tag{12}$$

where

$$\mathbf{K}=\begin{bmatrix} 1 & 0 & 1 & 0 & 0 & 0 & 0 & 0 \\ 0 & 1 & 0 & 1 & 0 & 0 & 0 & 0 \\ -1 & 0 & 1 & 0 & 0 & 0 & 0 & 0 \\ \lambda & -1 & \lambda & 1 & \lambda & 0 & \lambda & 0 \\ 0 & 0 & 0 & 0 & 1 & 0 & 1 & 0 \\ 0 & 0 & 0 & 0 & 0 & 1 & 0 & 1 \\ 0 & 0 & 0 & 0 & -1 & 0 & 1 & 0 \\ \lambda & 0 & \lambda & 0 & \lambda & -1 & \lambda & 1 \end{bmatrix} \tag{13}$$

$$\mathbf{H}=\begin{bmatrix} \cos(\beta a) & \sin(\beta a) & \cosh(\beta a) & \sinh(\beta a) & 0 & 0 & 0 & 0 \\ -\sin(\beta a) & \cos(\beta a) & \sinh(\beta a) & \cosh(\beta a) & 0 & 0 & 0 & 0 \\ -\cos(\beta a) & -\sin(\beta a) & \cosh(\beta a) & \sinh(\beta a) & 0 & 0 & 0 & 0 \\ \sin(\beta a) & -\cos(\beta a) & \sinh(\beta a) & \cosh(\beta a) & 0 & 0 & 0 & 0 \\ 0 & 0 & 0 & 0 & \cos(\beta a) & \sin(\beta a) & \cosh(\beta a) & \sinh(\beta a) \\ 0 & 0 & 0 & 0 & -\sin(\beta a) & \cos(\beta a) & \sinh(\beta a) & \cosh(\beta a) \\ 0 & 0 & 0 & 0 & -\cos(\beta a) & -\sin(\beta a) & \cosh(\beta a) & \sinh(\beta a) \\ 0 & 0 & 0 & 0 & \sin(\beta a) & -\cos(\beta a) & \sinh(\beta a) & \cosh(\beta a) \end{bmatrix} \tag{14}$$

$$\lambda=\frac{mk\omega^2}{(m\omega^2-2k)EI\beta^3} \tag{15}$$

For the infinitely periodic model, the Bloch's theorem implies that $\boldsymbol{\psi}_n = e^{\mathrm{j}qa}\boldsymbol{\psi}_{n-1}$, in which q denotes the Bloch wave number. Therefore, the standard eigenvalue problem of transfer matrix $\mathbf{T}$ from Eq. (12) is obtained

$$\left|\mathbf{T}-e^{\mathrm{j}qa}\mathbf{I}\right|=0 \tag{16}$$

where $\mathbf{I}$ is the 8×8 unit matrix.

2.3. Finite element model

In order to validate the derived theoretical model that implies simplifying the truss core with lumped parameters, a finite element model of the metamaterial sandwich beam (MSB) is developed for comparison. For the infinitely long model, to obtain the band structure with FEM, the standard procedure is first developing the model of one unit cell, then applying the periodic boundary condition by using the Bloch's theorem which gives Eq. (17), and finally seeking the eigenfrequencies of the general eigenvalue problem

$$\mathbf{u}_n(\boldsymbol{r})=\mathbf{u}_{n-1}(\boldsymbol{r}+\boldsymbol{R})\,e^{-i\boldsymbol{k}\cdot\boldsymbol{R}} \tag{17}$$

where $\boldsymbol{r}$ is the general coordinate, $\mathbf{u}_n$ denotes the general displacement, the subscript n denotes the n-th cell, $\boldsymbol{k}$ is the wave number vector, $\boldsymbol{R}$ is the lattice constant vector. In the study of this paper, only the flexural vibration of the sandwich beam is considered. The problem is thus degenerated into a one-dimensional case, in which $\boldsymbol{r}$ is the horizontal direction coordinate x, $\mathbf{u}_n$ defines the MSB deflection, $\boldsymbol{k}$ is the scalar wave number q, and $\boldsymbol{R}$ corresponds to the scalar lattice constant a. However, the utilization of the Bloch's theorem produces a set of complex valued constraint equations (Eq. (17)) which is difficult to be handled by the commercial FEM package. To enable the utilization of common commercial FEM package for the calculation of band structures, Åberg and Gudmundson [58] proposed a general solution to address the problem. The key is to first express $\mathbf{u}_n(\boldsymbol{r})$ in following form

$$\mathbf{u}_n(\boldsymbol{r})=\mathrm{Re}\left(\mathbf{u}_n(\boldsymbol{r})\right)+\mathrm{j}\cdot\mathrm{Im}\left(\mathbf{u}_n(\boldsymbol{r})\right) \tag{18}$$

where the superscript Re and Im represent the real and imaginary components, respectively. Then, splitting complex valued constraint equations into real and imaginary parts

$$\begin{cases} \mathrm{Re}\left(\mathbf{u}_n(\boldsymbol{r})\right)=\mathrm{Re}\left(\mathbf{u}_n(\boldsymbol{r}+\boldsymbol{R})\right)\cos\left(\boldsymbol{k}\cdot\boldsymbol{R}\right)+\mathrm{Im}\left(\mathbf{u}_n(\boldsymbol{r}+\boldsymbol{R})\right)\sin\left(\boldsymbol{k}\cdot\boldsymbol{R}\right) \\ \mathrm{Im}\left(\mathbf{u}_n(\boldsymbol{r})\right)=\mathrm{Im}\left(\mathbf{u}_n(\boldsymbol{r}+\boldsymbol{R})\right)\cos\left(\boldsymbol{k}\cdot\boldsymbol{R}\right)+\mathrm{Re}\left(\mathbf{u}_n(\boldsymbol{r}+\boldsymbol{R})\right)\sin\left(\boldsymbol{k}\cdot\boldsymbol{R}\right) \end{cases} \tag{19}$$

Table 1
The material properties and geometric dimensions of the hourglass truss structure.

E (Gpa)	ρ (kg/m^3)	l (mm)	r_c (mm)	α (°)	m (kg)
210	7930	35.35	1	45	0.04

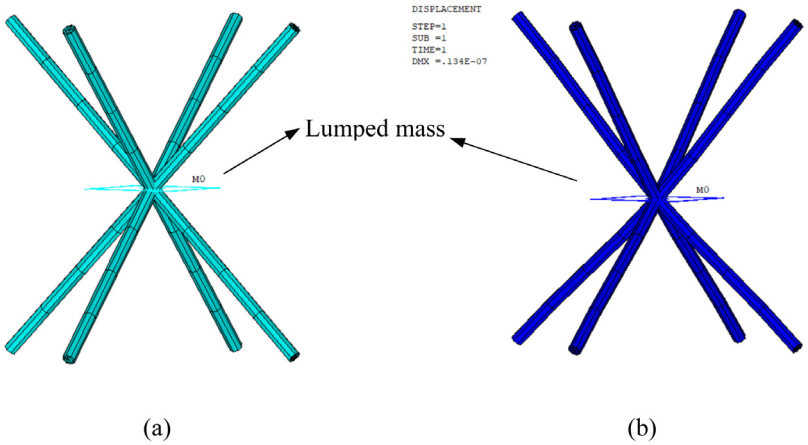

Fig. 5. ANSYS model of the hourglass structure with a lumped mass (a) without deformation (b) with deformation under an external force.

In the commercial software ANSYS, the above mentioned procedures can be implemented by using the CE function to define constraint equations described by Eq. (19) for relating degrees of freedom of the nodes at the boundaries. Finally, with the provided modal analysis function, by sweeping the wave number $\boldsymbol{k}$ (i.e., q in the present case), one obtains the solution for the eigenfrequency. Plotting the solved eigenfrequency versus the wave number gives the band structure of the sandwich metamaterial beam. Regarding the finitely long model, the procedure for obtaining the transmittance is quite straightforward and there is no need to elaborate the details. In the following FEM simulations presented in this study, 4-node shell element SHELL181 is used to model the face sheets, 3-dimensional 3-node beam element BEAM189 is used to model the struts, 2-node element COMBIN14 is selected to model the springs and 1-node element MASS21 is selected to model the lumped mass in the truss core.

3. Model validation

3.1. Validation of the equivalent stiffness of the hourglass truss structure

The theoretical result for the equivalent stiffness of the hourglass truss structure is validated by FEM. The proposed hourglass truss structure model is built in ANSYS as shown in Fig. 5(a). The ends of all the struts are clamped, a lumped mass is added on the intersection of the eight oblique struts and an external unit force is applied on the lumped mass in y-direction. The relevant material properties and geometric dimensions are given in Table 1.

From the results of FEM as shown in Fig. 5(b), the displacement of the intersection of the eight struts under an external unit force is 1.34×10^{-8} m. The equivalent stiffness in y-direction calculated is thus 3.73×10^{7} N/m, and the result obtained for $2k$ by Eq. (7) is also 3.73×10^{7} N/m. Thus, the analytical result of the equivalent stiffness of hourglass truss structure is confirmed. It is worth mentioning that the equivalent stiffness of the oblique struts was derived by neglecting the bending effect under the assumption of small deformation. The bending of the strut in Fig. 5(b) looks non-negligible, only because the displacement field is intentionally magnified to provide a clear illustration of the deformation of the struts. Since the total mass of the struts is small, a lumped mass is introduced to enlarge the band gap and tune it to the low-frequency range. Similar to the problem of a cantilever beam system, around the fundamental resonance, the equivalent mass of a plain beam is approximately 0.24 times of its static mass. If a relatively large tip mass is introduced, the tip mass will play the dominant role, and the equivalent mass of the plain beam itself becomes negligible. In our study, the lumped mass is relatively much larger (about 6 times) than the mass of the struts. Therefore, the mass of the struts could be neglected in the modelling.

3.2. Validation of band structures of MSB

3.2.1. Comparison of MDB & CMB models

To demonstrate the equivalence of metamaterial dual-beam (MDB) and conventional metamaterial beam (CMB) models under base excitation, band gaps of MDB and CMB are calculated and compared by using the TMM, together with the

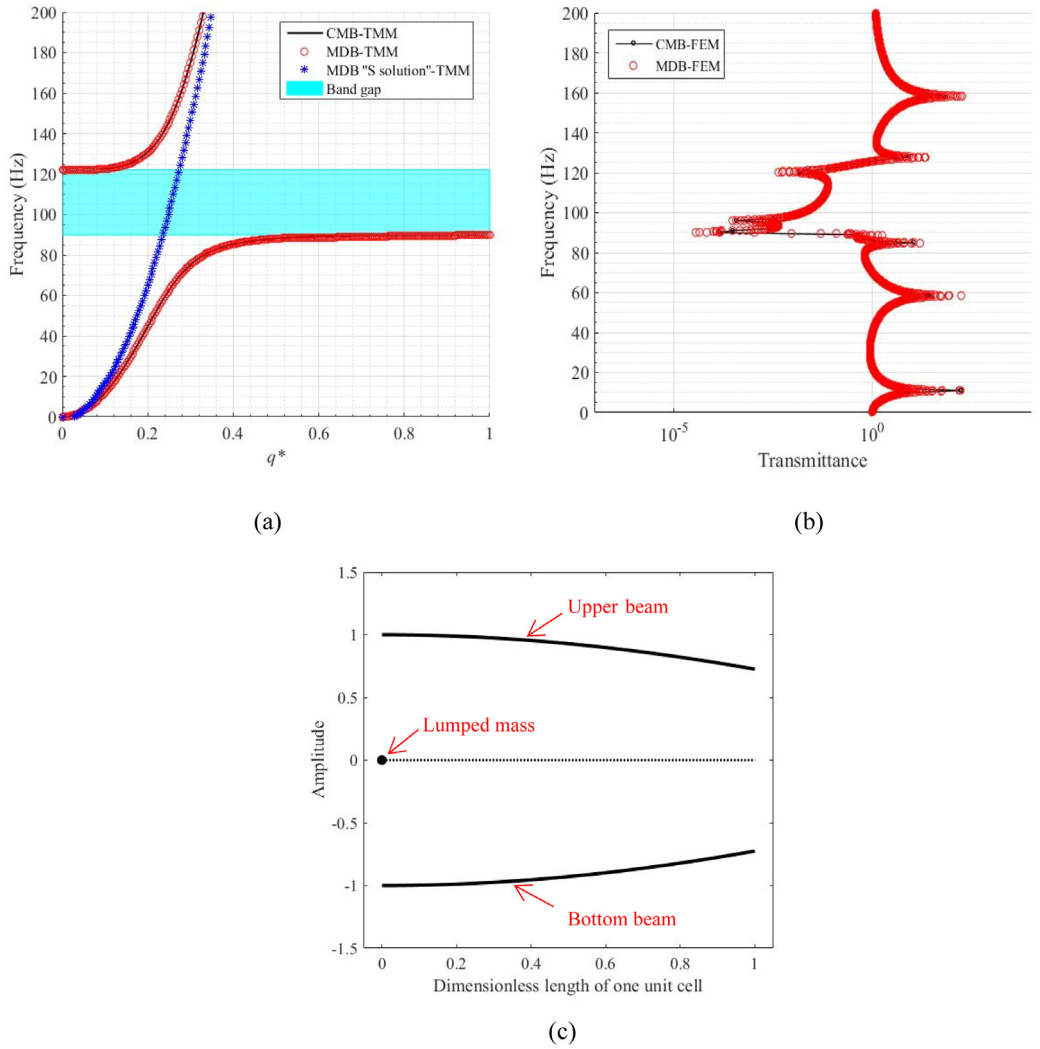

Fig. 6. (a) Band structures of MDB and CMB calculated by TMM, (b) transmittances of MDB and CMB calculated by FEM, (c) vibration mode of one unit cell of the infinitely long MDB at 95 Hz calculated by TMM.

transmittances of the two finitely long models by FEM. The dimensions and material parameters used in the calculation come from CMB in the published literature [59]. In the MDB model, the total stiffness of two springs and the total thickness of two beams are equal to the spring stiffness and beam thickness of the CMB.

As shown in Fig. 6(a), apart from a set of solutions denoted as blue stars, the band gap of MDB agrees well with that of CMB. Those solutions denoted as blue stars and termed as "S solution" represent the symmetric mode solutions when two beams move exactly in the opposite directions and the resonators keep stationary during vibration, which, however, will not appear when the beams are subjected to base excitation. Though the MDB model has the symmetric vibration mode, under the given base excitation condition (i.e., the two beams of the MDB model are clamped to the same base) the symmetric vibration mode can never be stimulated. Only the asymmetric modes when the top and bottom beams have exactly the same deflections will be stimulated. To help understand why the symmetric mode cannot be stimulated, for simplicity but without loss of generality, a 3-DOF system with the same symmetric characteristic is discussed in Appendix. For the MDB model, the symmetric vibration mode of one unit cell of the infinitely long MDB is shown in Fig. 6(c). Those solutions corresponding to the symmetric mode do not exist for the CMB with a single host beam. Furthermore, finite element models of the finitely long MDB and CMB are built in ANSYS to verify the predictions of the band gaps by TMM, as shown in Fig. 6(b). A base excitation is applied at the clamped end of the MDB and the CMB, and the displacements at the free ends are calculated. As expected, the transmittances demonstrate the existence of the band gap in the frequency range of about 90–122 Hz. Also, it is noted that the transmittances of the MDB and CMB are consistent. In addition, there is no "S solution" in the transmittance results since the MDB is subjected to base excitation. Based on these results, we can confirm that the CMB and MDB model are equivalent under base excitation.

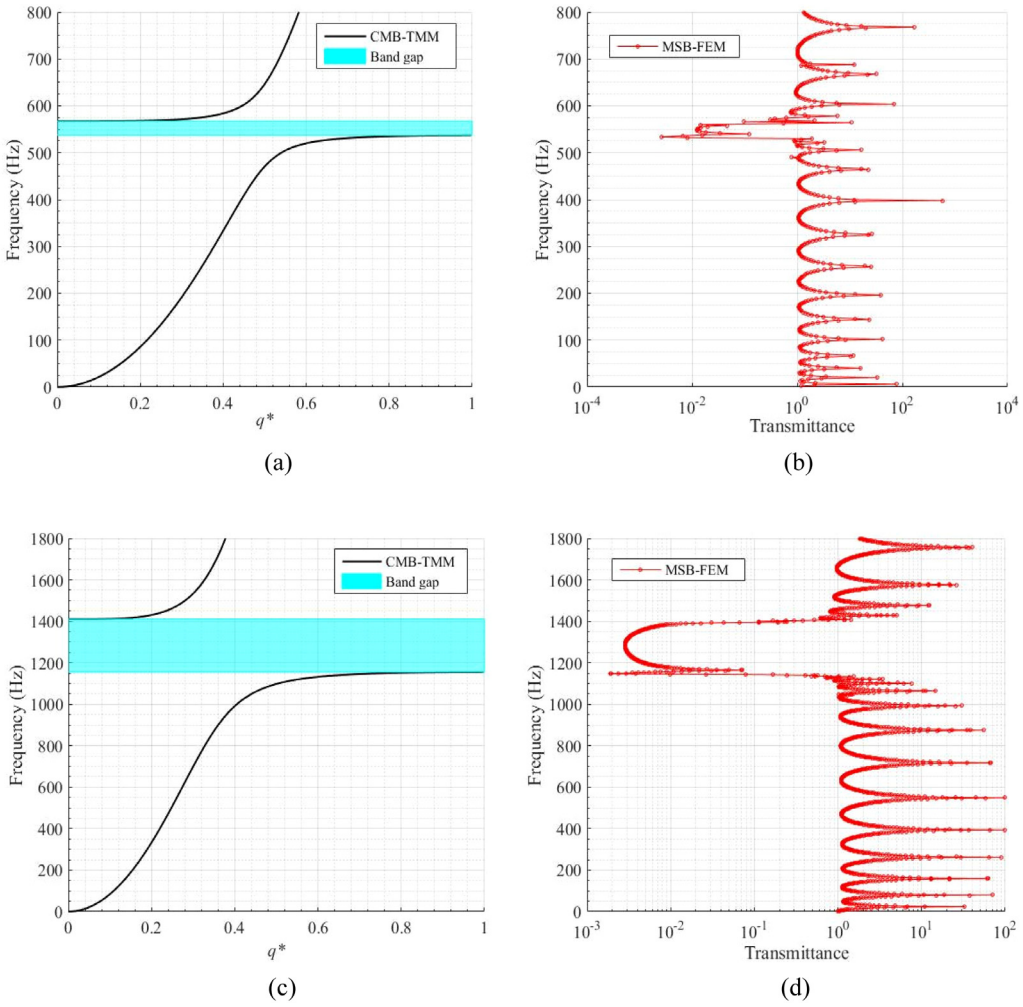

Fig. 7. (a) Band structure of the CMB by the TMM, (b) transmittance of the MSB by FEM with $\alpha = 25°$, $a = 160$ mm; (c) band structure of the CMB by the TMM, (b) transmittance of the MSB by FEM with $\alpha = 45°$, $a = 75$ mm, $r_c = 1$ mm, $h_f = 15$ mm and $h_c = 75$ mm.

The stiffness and mass of the local resonator are 1.2663×10^4 N/m and 0.0396 kg, respectively, which implies that the natural frequency of the local resonator is 90 Hz. To ease the comparison of the band gap predicted by various models presented in the literature, non-dimensionalization methods can be employed to reveal the intrinsic characteristic properties of the band gap. One commonly used non-dimensionalized band gap width is defined as the quotient between the band gap width and the natural frequency of the local resonator. In accordance with this definition, the dimensionless band gap width for the case presented in Fig. 6(a) can be calculated as 0.36, which is smaller than 1.04 from the metamaterial beam with multiple local resonators [22].

3.2.2. Comparison of MSB & CMB models

Since we simplified the metamaterial sandwich beam (MSB) as the metamaterial dual-beam (MDB) by using the equivalent stiffness of the hourglass truss core and we noted that the conventional metamaterial beam (CMB) and the MDB are equivalent under base excitation, we will further prove that the MSB can be represented by the CMB model. If this can be proved, the internal complexity (such as, pyramid truss core and hourglass truss core) of the MSBs can be significantly simplified and the existing theory and methods for the CMB can be utilized in the analysis of the MSB.

In the following validation, wood is selected to be the mother material. Band structure of the CMB model, representing the MSB, is calculated by the TMM. Meanwhile, the transmittance of the finitely long MSB model is also calculated by FEM to compare with and verify the predicted band gap. Fig. 7(a) and Fig. 7(c) show the band structures of the CMB model with α being 25° and 45°, respectively, in which the radius of struts r_c is 1 mm, the thickness of face sheets h_f is 15 mm and the thickness of core layer h_c is 75 mm. The band gaps appear in the frequency ranges of 537–568 Hz and 1151–1411 Hz, respectively. Fig. 7(b) and Fig. 7(d) show the transmittances of the MSB predicted by FEM. It is observed the predictions of the transmittance and band gaps are in good agreement.

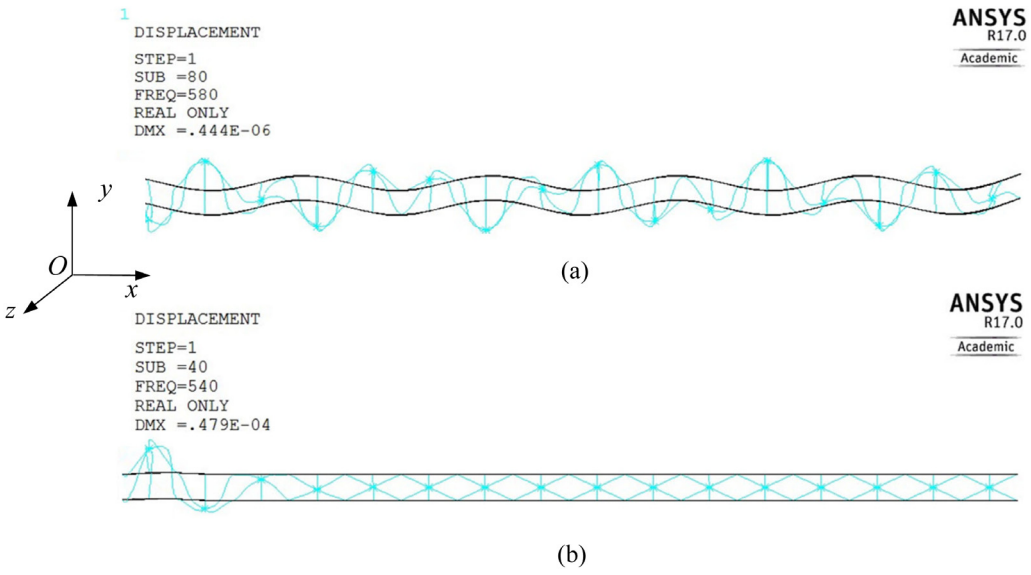

Fig. 8. Vibration modes of the finitely long MSB under harmonic response (a) out of band gap frequency range, (b) within band gap frequency range with $\alpha = 25°$, $a = 160$ mm, $r_c = 1$ mm, $h_f = 15$ mm and $h_c = 75$ mm.

Fig. 8(a) and (b) show the vibration modes of the finitely long MSB under harmonic response analysis for same parameters as those used in Fig. 7(b), in which the former is the vibration amplitude outside the frequency range of the band gap (580 Hz) and the latter is the vibration amplitude within the frequency range of the band gap (540 Hz). It can be seen that the truss structures between the two face sheets have not only transverse component of motion in y-direction, but also longitudinal motion in x-direction. Existence of these longitudinal vibrations can lead to some mismatch between the analytical and simulation results. Several resonators appear to move outside the two face sheets during vibration. In fact, the resonators are not truly penetrating the physical boundaries. The displacement field is magnified by a scaling factor of 288023 in ANSYS to illustrate the elastic deformation clearly. Since the relative displacement between the resonator and the host beam is magnified, while the geometric dimensions are at the true scale, the result becomes visually distorted. Putting aside this issue, from Fig. 8, it can be observed that when the excitation frequency falls into the band gap, the transverse displacement dramatically decreases along the host beam. In other words, the vibration of the host beam is significantly suppressed.

To further demonstrate that the MSB can be represented by the CMB model, the band structure is also directly calculated by FEM using an infinitely long model of the MSB. Fig. 9 shows the dispersion relations of the MSB with hourglass lattice truss core computed by FEM compared with that of the CMB by TMM, and the material and dimension parameters are the same as those from Fig. 7(d). It is concluded that the relative errors of the band gap between FEM and TMM are acceptable, which verifies the effectiveness of the analytical model in-depth. Although the hourglass truss structure has various vibration modes as shown by dotted lines in the figure, only the transverse mode in y-direction plays the dominant role under base excitation.

To understand the different types of waves for the MSB which do not exist in the simplified CMB model, modal analysis is conducted and the modes at four points P_1, P_2, P_3 and P_4 in Fig. 9 are shown in Fig. 10. At point P_1, the dispersion branch is associated with the transverse vibration mode as shown in Fig. 10(a) which implies the wave is flexural. In comparison, Fig. 10 (b) and (c) show the torsional and longitudinal waves, respectively, for points P_2 and P_3. For point P_4, the symmetric vibration mode for the two face sheet beams is observed (Fig. 10(d)), which corresponds to the "S solution" in Fig. 5(c). The complexity of the internal form of the MSB leads to various vibration modes. Though the torsional, longitudinal and symmetric modes do exist and could be excited given a particular excitation, only the transverse vibration mode dominates under base excitation, which can be proved by the clear gap in Fig. 7(b) and (d), i.e., no other modes occur in the gap.

From the results given above, it is confirmed that the oblique struts can be simplified as vertical springs in the proposed model and the MSB can indeed be approximated as the CMB. Thus, in the next section for the parametric study, the analytical results are obtained by using the CMB model to simplify the calculation process.

4. Parametric study

The metamaterial sandwich beam (MSB) with hourglass lattice truss core has a complicated internal composition that makes it multifunctional. The parametric study for sandwich structures is necessary to achieve specific properties in

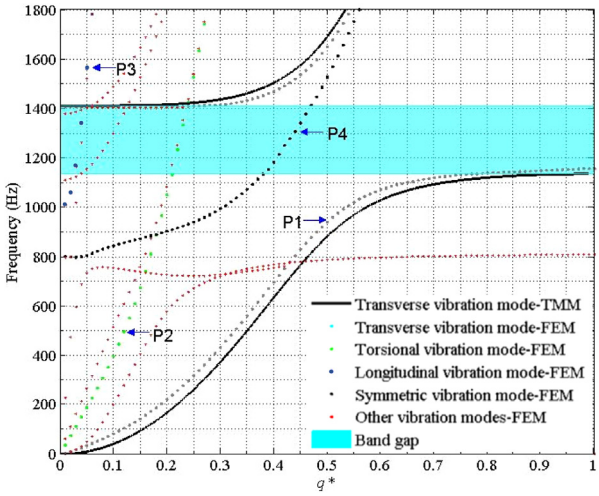

Fig. 9. Band structure of MSB calculated by FEM and band structure of CMB calculated by TMM with $\alpha = 45°$, $a = 75$ mm, $r_c = 1$ mm, $h_f = 15$ mm and $h_c = 75$ mm.

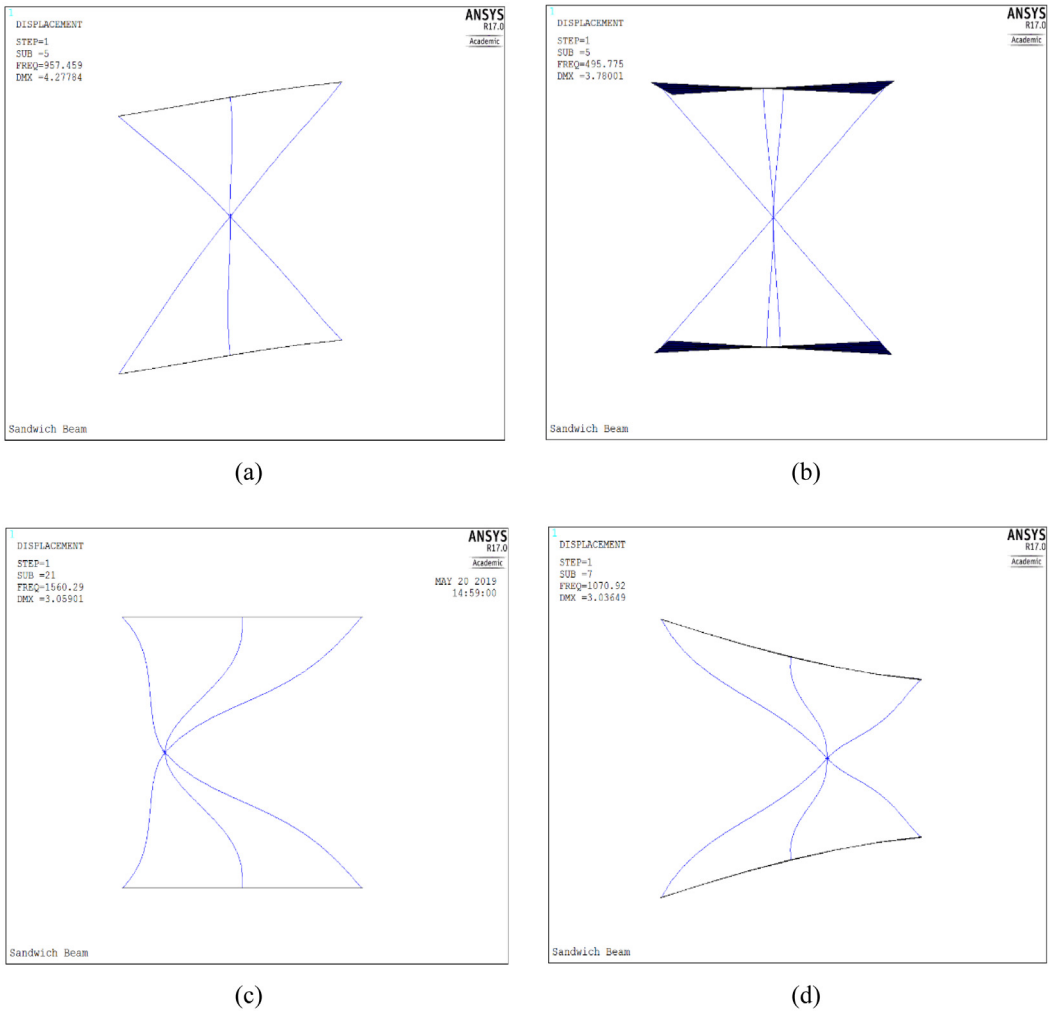

Fig. 10. Vibration modes at points: (a) P_1, (b) P_2, (c) P_3 and (d) P_4.

Table 2
Material properties of MSB.

Material	Elastic modulus (GPa)	Poisson's ratio	Density (kg/m^3)
Wood	9	0.4	500
Aluminium	69	0.32	2700

structural design. Effects of h_c, d, h_f and r_c on band structures of the MSB with different materials are investigated. Wood and Aluminium have been widely used in architecture, aerospace, marine and other engineering fields, and their material properties are given in Table 2, respectively [60,61].

As confirmed in the previous section, the MSB can be represented by the conventional metamaterial beam (CMB) model for the simplified theoretical analysis to obtain the band gaps using TMM. The results are compared with those predicted from the transmittance of the MSB modelled by FEM, as plotted in Fig. 11, where h_c is 75 mm, while r_c and h_f are varied. The corresponding results are presented in the three sub-figures, respectively. It is noted that d is changed by varying α. It is found that for the wood material, the results by the TMM for the CMB model and FEM for the MSB are more consistent than the results for the aluminium material. In addition, increasing r_c, the inconsistency between the two models become more obvious. There are a few reasons for the band gaps of the MSB obtained by FEM to be lower than those from the analytical results for the CMB model by TMM. First, increasing r_c implies increasing mass of the truss that inevitably increases the effective mass of the resonators and decreases their natural frequency, which, however, is neglected in the analytical model. Second, there exists a relative displacement between the struts of every unit cell which leads to coupled bending–twisting modes that implies decreasing the overall stiffness of the truss structure. However, the relative errors between the two models are still lower than 3% in the relatively high frequency ranges. This data proves that the proposed model of the MSB is applicable for different materials. The location of the band gaps mainly depends on the Young's modulus of the material. The smaller the Young's modulus, the lower the band gap frequency. In addition, smaller d leads to wider band gaps but in a higher frequency range.

It should also be mentioned that, for the results shown in Fig. 11, h_f is increased along with r_c. It is easily understood that in the CMB, the smaller the thickness of the host beam, the wider the frequency band gap. However, the difference between the MSB with hourglass lattice truss core and the simplified CMB model is that for the former, there are some limitations for the relation between r_c and h_f. Fig. 12 shows vibration of the MSB from the harmonic response analysis in FEM under base excitation, and the structural parameters are the same as those of Fig. 7(b), except that h_f is 5 mm. It is observed that there exists a severe twisting of the two face sheet beams about the longitudinal axis if they are very thin, because the overall bending stiffness of the struts is not negligibly small compared to the thin face sheets. The twisting phenomenon will certainly increase the inconsistency between the MSB model using FEM and the simplified CMB model by TMM. Therefore, h_f should be increased as r_c increases for obtaining sensible prediction of the band gaps.

Fig. 13 shows the effect of h_c on band gaps of the wood and aluminium MSBs in which r_c, h_f and a are 1 mm, 15 mm, 75 mm, respectively. We note that h_c is varied by changing α and length of the strut, i.e., h_c=2$l$sin α. As h_c increases from 20 mm to 150 mm, it is noted that the band gaps for the wood and aluminium MSBs first move to the higher frequency ranges and then decline a bit with h_c continuously increasing. The widths of the band gaps are first broadened, reach the maximum and then decline a bit. It can be concluded from Eq. (7) that the equivalent stiffness is first increased and then decreased as h_c increases, since both α and l_{HB} are changing, which makes the resonant frequency increase first and decline later. According to [34], the ending frequency of LR band gap is given as $\omega_{eL} = \omega_r\sqrt{(1 + m/2\rho Aa)}$, where ω_r is the natural frequency of the resonators, and the width of the band gap is also directly related to ω_r. Thus, by tuning h_c reasonably, appropriate band gaps can be obtained.

Fig. 14 shows the effect of r_c on the band gaps of the wood and aluminium MSBs in which α, h_c, h_f and d are 45°, 75 mm, 20 mm and 75 mm, respectively. It is noted that with the increase of r_c, the band gaps of both wood and aluminium MSBs move to the higher frequency range, and the band gap widths become larger. This is because increasing r_c inevitably increases the equivalent stiffness of the hourglass truss core, which increases the natural frequency of the resonators.

Fig. 15 shows the effect of h_f on band gaps of the MSBs in which α, h_c, r_c and d are 45°, 75 mm, 1 mm and 75 mm, respectively. It is noted that with other parameters fixed, increasing h_f will weaken the wave attenuation in the MSB. As h_f increases, the widths of the band gaps of MSBs become narrower because they are directly related to the ratio of the mass of the resonators to the weight of the host beams [62]. The locations of band gaps will not move since they mainly depend on the natural frequency of the resonators, while the equivalent stiffness and lumped mass do not change in this case.

5. Conclusions

Though the research in the existing literature has already proposed sandwich beam based metamaterials, most of them only considered sandwiches with homogenized cores and the local resonators were often modelled with lumped parameters. This study has proposed a novel metamaterial sandwich beam (MSB) using truss core sandwiches. The local

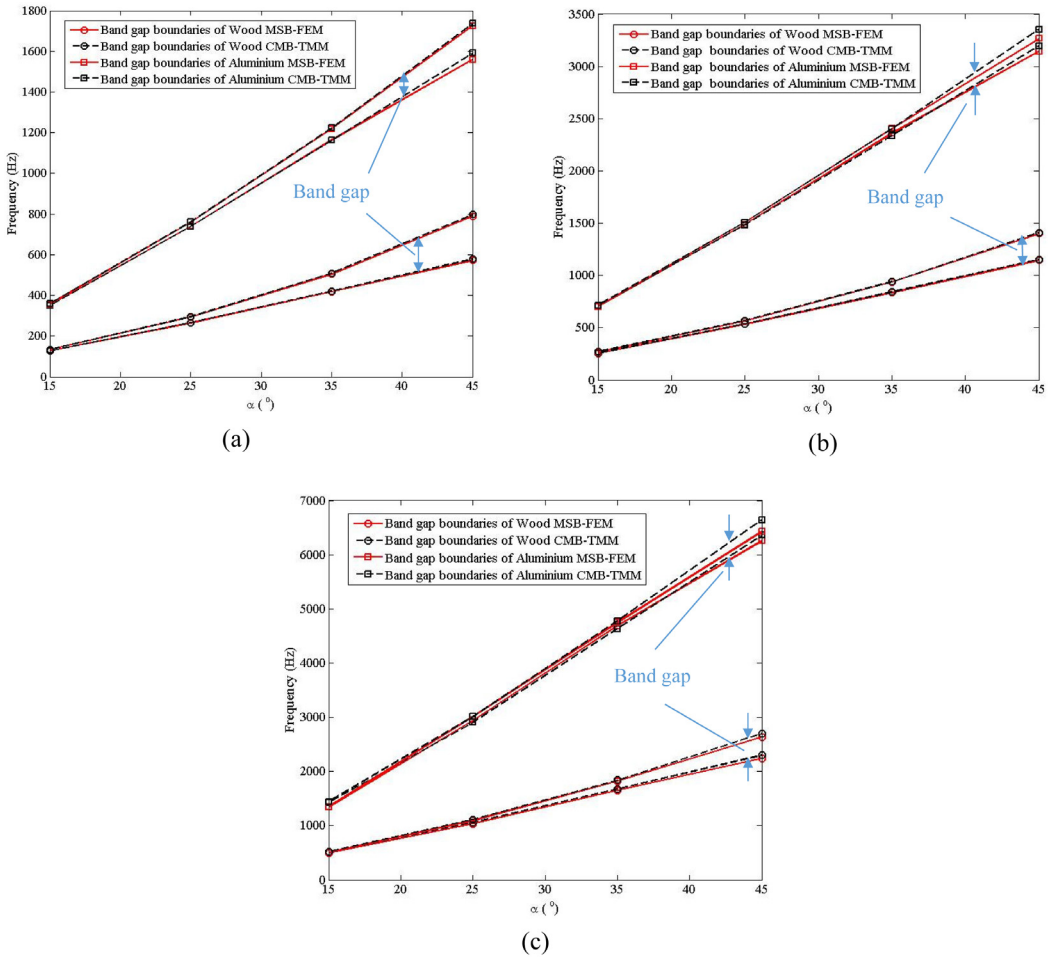

Fig. 11. Band gaps of CMB and MSB with different materials with (a) $r_c = 0.5$ mm, $h_c = 75$ mm $h_f = 8$ mm, (b) $r_c = 1$ mm, $h_c = 75$ mm, $h_f = 15$ mm, and (c) $r_c = 2$ mm, $h_c = 75$ mm, $h_f = 20$ mm.

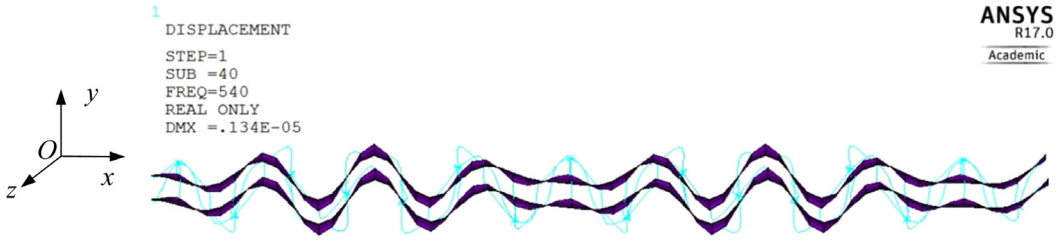

Fig. 12. Vibration modes of the MSB under harmonic response analysis with α =25°, $a = 160$ mm, $r_c = 1$ mm, $h_f = 5$ mm and $h_c = 75$ mm.

resonators are realized using the readily existed hourglass truss structures. The proposed MSB is expected to be a more realistic model. A methodology is developed for modelling the proposed MSB model. The truss structure loaded with a concentrated mass is simplified to a spring–mass–spring system (i.e., 'local resonator') for which the equivalent stiffness is derived using Hook's law. It is found that the equivalent stiffness of the truss structure is dependent on the length, the cross-sectional area and the inclination angle of the struts. Based on the lumped parameterization of the truss structure, the MSB is reduced to the metamaterial dual-beam (MDB) model and then represented by the conventional metamaterial beam (CMB) model. This equivalent representation method is validated by FEM through both a transmittance analysis and a band structure analysis. The effects of the material and geometric parameters on the band structures of the MSB are investigated by a parametric study. It is discovered that with the increase of h_c, the band gaps move to higher frequencies and are widened until reaching a maximum, since the equivalent stiffness of the 'local resonator' is first increased then

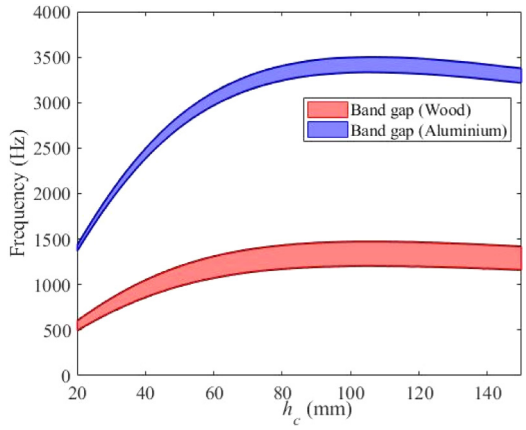

Fig. 13. Effect of h_c on band gaps of the MSBs with $a = 75$ mm, $r_c = 1$ mm and $h_f = 15$ mm.

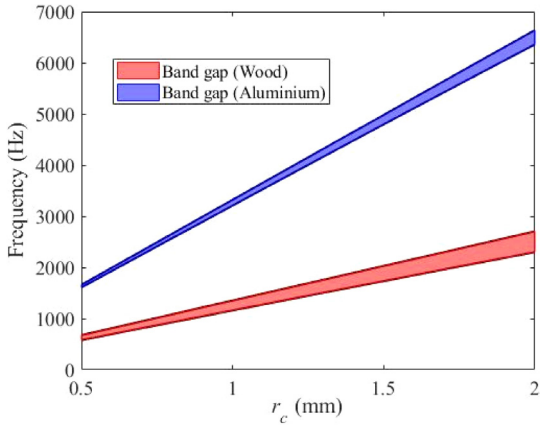

Fig. 14. Effect of r_c of struts on band gaps of the MSBs with α =45°, $a = 75$ mm, $h_c = 75$ mm and $h_f = 20$ mm.

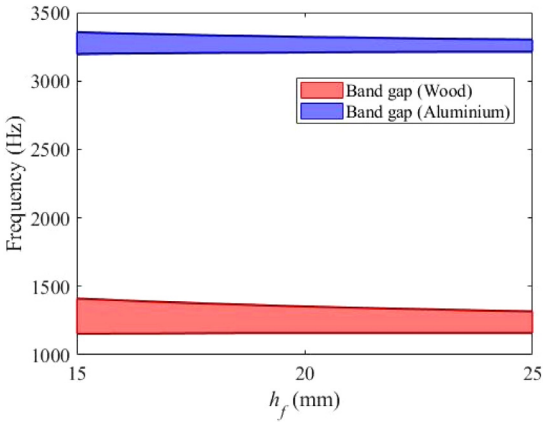

Fig. 15. Effect of h_f on band gaps of the MSBs with $\alpha = 45°$, $a = 75$ mm, $h_c = 75$ mm and $r_c = 1$ mm.

decreased as h_c increases. Increasing r_c broadens the band gaps and makes them move to higher frequencies, because increasing r_c increases the equivalent stiffness, thus the natural frequency of the 'local resonator'. On the contrary, the increase of h_f makes the band gaps narrower, due to the decrease of the mass ratio between the 'local resonator' and the host beam. In conclusion, this work provides a roadmap of modelling of lightweight lattice sandwich beams with complex core structures and presents guidelines for applications of such beams to control wave propagation.

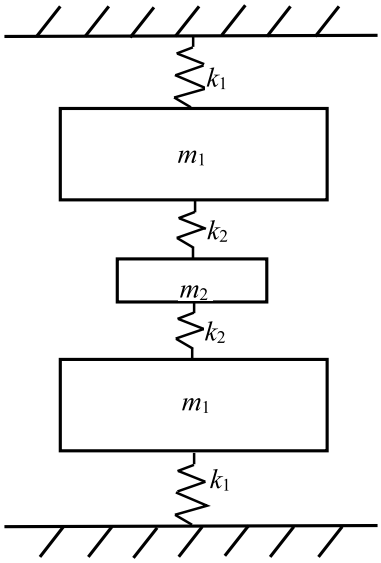

Fig. A.1. Diagram of a 3-DOF system with a symmetric vibration mode.

CRediT authorship contribution statement

Zhenkun Guo: Conceptualization, Prototype design, Writing - original draft, Methodology, Analytical analysis. **Guobiao Hu:** Conceptualization, Prototype design and manufacture, Results discussion. **Vladislav Sorokin:** Supervision, Review and editing, Methodology, Results discussion, Proof-reading. **Lihua Tang:** Supervision, Writing - review & editing, Methodology, Results discussion, Proof-reading. **Xiaodong Yang:** Review and editing, Results discussion, Methodology, Proof-reading, Funding acquisition. **Jun Zhang:** Review and editing, Results discussion, Proof-reading, Funding acquisition.

Declaration of competing interest

The authors declare that they have no known competing financial interests or personal relationships that could have appeared to influence the work reported in this paper.

Acknowledgements

This study is financially supported by the scholarship from China Scholarship Council (no. 201806540003), National Natural Science Foundation of China (Project no. 11672007, 11290152, 51775031) and Beijing Natural Science Foundation, China (Project no. 8202015).

Appendix

Fig. A.1 shows the schematic of a 3-DOF system that is featured with the mirror symmetry characteristic. This 3-DOF system has a symmetric vibration mode. For the free vibration of the 3-DOF system as shown in Fig. A.1, the governing equations can be written as:

$$\begin{cases} m_1\ddot{x}_1 + k_1x_1 + k_2\,(x_1 - x_2) = 0 \\ m_2\ddot{x}_2 + k_2\,(2x_2 - x_1 - x_3) = 0 \\ m_1\ddot{x}_3 + k_1x_3 + k_2\,(x_3 - x_2) = 0 \end{cases} \tag{A.1}$$

Without loss of generality but just to facilitate the following calculation, we assume that $m_1 = m$, $m_2 = m/2$, $k_1 = k$, $k_2 = k/5$. x_1, x_2 and x_3 denote the displacements of the three DOFs, respectively. The governing equations can be re-expressed in the matrix form as:

$$\mathbf{m}\ddot{\mathbf{x}} + \mathbf{k}\mathbf{x} = 0 \tag{A.2}$$

where $\mathbf{m} = \begin{bmatrix} m & 0 & 0 \\ 0 & \frac{1}{2}m & 0 \\ 0 & 0 & m \end{bmatrix}$ and $\mathbf{k} = \begin{bmatrix} \frac{6}{5}k & -\frac{1}{5}k & 0 \\ -\frac{1}{5}k & \frac{2}{5}k & -\frac{1}{5}k \\ 0 & -\frac{1}{5}k & \frac{6}{5}k \end{bmatrix}$.

The natural frequencies of the 3-DOF system can be obtained through a modal analysis.

$$\begin{cases} \omega_1 = \dfrac{\sqrt{5\left(5-\sqrt{5}\right)}}{5}\sqrt{\dfrac{k}{m}} \\ \omega_2 = \dfrac{\sqrt{30}}{5}\sqrt{\dfrac{k}{m}} \\ \omega_3 = \dfrac{\sqrt{5\left(5+\sqrt{5}\right)}}{5}\sqrt{\dfrac{k}{m}} \end{cases} \tag{A.3}$$

For the first vibration mode, we can obtain $\mathbf{X}^{(1)} = X_1^{(1)} \begin{bmatrix} 1 \\ 1+\sqrt{5} \\ 1 \end{bmatrix}$. It can be noted that m_1 and m_3 always have the exactly same motion, and m_2 undergoes in-phase motion. For the second vibration mode, we have $\mathbf{X}^{(2)} = X_1^{(2)} \begin{bmatrix} 1 \\ 0 \\ -1 \end{bmatrix}$. It can be seen that m_2 keeps stationary, while m_1, m_3 are doing mirror movements with the same displacement amplitude but in opposite directions. The second vibration mode is the aforementioned symmetric vibration mode. For the third vibration mode, it can be obtained that $\mathbf{X}^{(3)} = X_1^{(3)} \begin{bmatrix} 1 \\ 1-\sqrt{5} \\ 1 \end{bmatrix}$. Similar to the first vibration mode, m_1, m_3 have the exact same motion. The difference is that m_2 undergoes out-of-phase motion. For mass normalized mode shapes, we can derive that $X_1^{(1)} = \frac{1}{\sqrt{5+\sqrt{5}}\sqrt{m}}$, $X_1^{(2)} = \frac{1}{\sqrt{2}\sqrt{m}}$ and $X_1^{(3)} = \frac{1}{\sqrt{5-\sqrt{5}}\sqrt{m}}$.

After determining the natural frequencies and vibration modes of the 3-DOF system, we now proceed to the forced vibration analysis of the 3-DOF system. The governing equations can be written as:

$$\mathbf{m}\ddot{\mathbf{x}} + \mathbf{k}\mathbf{x} = \mathbf{f} \tag{A.4}$$

We assume a unified base excitation which means that m_1 and m_3 are connected to the foundations with the same displacement. The base excitation is assumed to be controlled at a constant acceleration level:

$$\mathbf{f} = \begin{bmatrix} -mA_{cc}\cos(\omega t) \\ -\frac{1}{2}mA_{cc}\cos(\omega t) \\ -mA_{cc}\cos(\omega t) \end{bmatrix} \tag{A.5}$$

Using the modal superposition method, the solution to Eq. (A.4) is assumed as $\mathbf{x}(t) = \mathbf{X}\mathbf{q}(t)$ in which $\mathbf{X} = \begin{bmatrix} \mathbf{X}^{(1)} & \mathbf{X}^{(2)} & \mathbf{X}^{(3)} \end{bmatrix}$ and $\mathbf{q}(t) = \begin{bmatrix} q_1(t) & q_2(t) & q_3(t) \end{bmatrix}^T$. Substituting the assumed solutions into Eq. (A.4) and using the orthogonality relation yields the modal governing equations:

$$\ddot{\mathbf{q}}(t) + \begin{bmatrix} \omega_1^2 & 0 & \\ 0 & \omega_2^2 & 0 \\ 0 & 0 & \omega_3^2 \end{bmatrix} \mathbf{q}(t) = \mathbf{Q} \tag{A.6}$$

where $\mathbf{Q} = \mathbf{X}^T\mathbf{f}$ is the vector of the modal excitation force. It can be easily derived that the value of the second element in the vector $\mathbf{Q}$ is always 0. Therefore, it can be concluded that under the unified base excitation we defined, the contribution of the second mode of the 3-DOF system, i.e., the symmetric mode, is always 0, which means that it cannot be excited. Note that if the base excitation is changed, for example, the top and bottom masses i.e., m_1 and m_3, are connected to different foundations undergoing different displacements, then it will be found that the second element in the vector $\mathbf{Q}$ is no longer 0, indicating that the symmetric mode is stimulated.

References

[1] G. Wang, et al., One-dimensional phononic crystals with locally resonant structures, Phys. Lett. A 327 (5–6) (2004) 512–521.

[2] M.M. Sigalas, E.N. Economou, Elastic and acoustic-wave band-structure, J. Sound Vib. 158 (2) (1992) 377–382.
[3] M.S. Kushwaha, et al., Acoustic band-structure of periodic elastic composites, Phys. Rev. Lett. 71 (13) (1993) 2022–2025.
[4] D.J. Mead, S. Markus, Coupled flexural longitudinal-wave motion in a periodic-beam, J. Sound Vib. 90 (1) (1983) 1–24.
[5] W. Elmadih, et al., Multidimensional phononic bandgaps in three-dimensional lattices for additive manufacturing, Materials 12 (11) (2019).
[6] M. Castaings, C. Bacon, Finite element modeling of torsional wave modes along pipes with absorbing materials, J. Acoust. Soc. Am. 119 (6) (2006) 3741–3751.
[7] F. Lucklum, M.J. Vellekoop, Bandgap engineering of three-dimensional phononic crystals in a simple cubic lattice, Appl. Phys. Lett. 113 (20) (2018).
[8] L. Brillouin, Wave propagation in periodic structures: electric filters and crystal lattices, 1953.
[9] M. Maldovan, Phonon wave interference and thermal bandgap materials, Nature Mater. 14 (7) (2015) 667–674.
[10] W. Elmadih, et al., Three-dimensional resonating metamaterials for low-frequency vibration attenuation, Sci. Rep. 9 (2019).
[11] D.L. Yu, et al., Flexural vibration band gaps in Timoshenko beams with locally resonant structures, J. Appl. Phys. 100 (12) (2006).
[12] H. Zhang, et al., Flexural wave band gaps in metamaterial beams with membrane-type resonators: theory and experiment, J. Phys. D: Appl. Phys. 48 (43) (2015).
[13] R.M. Delgado, Modelling of railway bridge-vehicle interaction on high speed tracks, Comput. Struct. 63 (3) (1997) 511–523.
[14] A. Erturk, J.M. Renno, D.J. Inman, Modeling of piezoelectric energy harvesting from an L-shaped beam-mass structure with an application to UAVs, J. Intell. Mater. Syst. Struct. 20 (5) (2009) 529–544.
[15] M. Ebrahimian, M.I. Todorovska, Wave propagation in a Timoshenko beam building model, J. Eng. Mech. 140 (5) (2013) 04014018.
[16] J.W. Hijmissen, W.T. van Horssen, On transverse vibrations of a vertical Timoshenko beam, J. Sound Vib. 314 (1–2) (2008) 161–179.
[17] G.J. Boertjens, W.T. van Horssen, An asymptotic theory for a weakly nonlinear beam equation with a quadratic perturbation, SIAM J. Appl. Math. 60 (2) (2000) 602–632.
[18] S.L. Zhou, F.M. Li, C.Z. Zhang, Vibration characteristics analysis of disordered two-span beams with numerical and experimental methods, J. Vib. Control 24 (16) (2018) 3641–3657.
[19] Y.Z. Liu, et al., Design guidelines for flexural wave attenuation of slender beams with local resonators, Phys. Lett. A 362 (5–6) (2007) 344–347.
[20] Y. Xiao, et al., Flexural wave propagation in beams with periodically attached vibration absorbers: Band-gap behavior and band formation mechanisms, J. Sound Vib. 332 (4) (2013) 867–893.
[21] Y. Xiao, J.H. Wen, X.S. Wen, Broadband locally resonant beams containing multiple periodic arrays of attached resonators, Phys. Lett. A 376 (16) (2012) 1384–1390.
[22] G.L. Huang, A chiral elastic metamaterial beam for broadband vibration suppression, J. Sound Vib. 333 (10) (2014) 2759–2773.
[23] P.F. Pai, H. Peng, S. Jiang, Acoustic metamaterial beams based on multi-frequency vibration absorbers, Int. J. Mech. Sci. 79 (2014) 195–205.
[24] H. Peng, P.F. Pai, H. Deng, Acoustic multi-stopband metamaterial plates design for broadband elastic wave absorption and vibration suppression, Int. J. Mech. Sci. 103 (2015) 104–114.
[25] T. Wang, M.-P. Sheng, Q.-H. Qin, Multi-flexural band gaps in an Euler–Bernoulli beam with lateral local resonators, Phys. Lett. A 380 (4) (2016) 525–529.
[26] T. Wang, et al., Flexural wave suppression by an acoustic metamaterial plate, Appl. Acoust. 114 (2016) 118–124.
[27] E. Miranda Jr, et al., Flexural wave band gaps in a multi-resonator elastic metamaterial plate using Kirchhoff–Love theory, Mech. Syst. Signal Process. 116 (2019) 480–504.
[28] L. D'Alessandro, et al., 3D Auxetic single material periodic structure with ultra-wide tunable bandgap, Sci. Rep. 8 (2018).
[29] A. Spadoni, M. Ruzzene, K. Cunefare, Vibration and wave propagation control of plates with periodic arrays of shunted piezoelectric patches, J. Intell. Mater. Syst. Struct. 20 (8) (2009) 979–990.
[30] S. Chen, et al., Wave propagation and attenuation in plates with periodic arrays of shunted piezo-patches, J. Sound Vib. 332 (6) (2013) 1520–1532.
[31] F.M. Li, C.Z. Zhang, Active localization of wave propagation in elastic beams using periodic placement of piezoelectric actuator/sensor pairs, J. Appl. Phys. 124 (8) (2018).
[32] C. Yilmaz, G.M. Hulbert, N. Kikuchi, Phononic band gaps induced by inertial amplification in periodic media, Phys. Rev. B 76 (5) (2007) 054309.
[33] M.B. Assouar, et al., Hybrid phononic crystal plates for lowering and widening acoustic band gaps, Ultrasonics 54 (8) (2014) 2159–2164.
[34] J.X. Zhou, et al., Local resonator with high-static-low-dynamic stiffness for lowering band gaps of flexural wave in beams, J. Appl. Phys. 121 (4) (2017).
[35] L. D'Alessandro, E. Belloni, G. D'Alo, L. Daniel, R. Ardito, A. Corigliano, F. Braghin, Modelling and experimental verification of a single phase three-dimensional lightweight locally resonant elastic metamaterial with complete low frequency bandgap, in: 11th International Congress on Engineered Materials Platforms for Novel Wave Phenomena (Metamaterials), 2017.
[36] X. Fang, et al., Ultra-low and ultra-broad-band nonlinear acoustic metamaterials, Nat. Commun. 8 (1) (2017) 1288.
[37] D. Mead, S. Markus, The forced vibration of a three-layer, damped sandwich beam with arbitrary boundary conditions, J. Sound Vib. 10 (2) (1969) 163–175.
[38] J. Reddy, N. Phan, Stability and vibration of isotropic, orthotropic and laminated plates according to a higher-order shear deformation theory, J. Sound Vib. 98 (2) (1985) 157–170.
[39] M. Ruzzene, P. Tsopelas, Control of wave propagation in sandwich plate rows with periodic honeycomb core, J. Eng. Mech. 129 (9) (2003) 975–986.
[40] L. Liu, K. Bhattacharya, Wave propagation in a sandwich structure, Int. J. Solids Struct. 46 (17) (2009) 3290–3300.
[41] J. Yang, et al., Vibration and damping characteristics of hybrid carbon fiber composite pyramidal truss sandwich panels with viscoelastic layers, Compos. Struct. 106 (2013) 570–580.
[42] X.X. Lyu, Active vibration control of lattice sandwich beams using the piezoelectric actuator/sensor pairs, Composites 67 (2014) 571–578.
[43] L.-Q. Chen, Vibration suppression of composite laminated plate with nonlinear energy sink, Acta Astronaut. 123 (2016) 109–115.
[44] Y.Z. Wang, Vibration band gap behaviors of sandwich panels with corrugated cores, Comput. Struct. 129 (2013) 30–39.
[45] J.S. Chen, C.T. Sun, Dynamic behavior of a sandwich beam with internal resonators, J. Sandw. Struct. Mater. 13 (4) (2011) 391–408.
[46] J.S. Chen, B. Sharma, C.T. Sun, Dynamic behaviour of sandwich structure containing spring-mass resonators, Compos. Struct. 93 (8) (2011) 2120–2125.
[47] B. Sharma, C.T. Sun, Local resonance and Bragg bandgaps in sandwich beams containing periodically inserted resonators, J. Sound Vib. 364 (2016) 133–146.
[48] J.S. Chen, Y.J. Huang, Wave propagation in sandwich structures with multiresonators, J. Vib. Acoust. Transact. ASME 138 (4) (2016).
[49] H. Chen, et al., Wave propagation and absorption of sandwich beams containing interior dissipative multi-resonators, Ultrasonics 76 (2017) 99–108.
[50] F.W. Zok, et al., A protocol for characterizing the structural performance of metallic sandwich panels: application to pyramidal truss cores, Int. J. Solids Struct. 41 (22–23) (2004) 6249–6271.
[51] J. Wang, et al., On the performance of truss panels with kagome cores, Int. J. Solids Struct. 40 (25) (2003) 6981–6988.

[52] V.S. Deshpande, N.A. Fleck, Collapse of truss core sandwich beams in 3-point bending, Int. J. Solids Struct. 38 (36–37) (2001) 6275–6305.
[53] L.-J. Feng, L.-Z. Wu, G.-C. Yu, An hourglass truss lattice structure and its mechanical performances, Mater. Des. 99 (2016) 581–591.
[54] K. Wei, et al., Mechanical Analysis and Modeling of Metallic Lattice Sandwich Additively Fabricated By Selective Laser Melting, Thin-Walled Structures, 2019, 106189.
[55] L.J. Feng, et al., Shear and bending performance of new type enhanced lattice truss structures, Int. J. Mech. Sci. 134 (2017) 589–598.
[56] S. Li, et al., Vibration behavior of metallic sandwich panels with Hourglass truss cores, Mar. Struct. 63 (2019) 84–98.
[57] Z.-K. Guo, X.-D. Yang, W. Zhang, Dynamic analysis, active and passive vibration control of double-layer hourglass lattice truss structures, J. Sandw. Struct. Mater. (2018) 1099636218784339.
[58] M. Åberg, P. Gudmundson, The usage of standard finite element codes for computation of dispersion relations in materials with periodic microstructure, J. Acoust. Soc. Am. 102 (4) (1997) 2007–2013.
[59] G.B. Hu, L.H. Tang, R. Das, Internally coupled metamaterial beam for simultaneous vibration suppression and low frequency energy harvesting, J. Appl. Phys. 123 (5) (2018).
[60] D.E. Kretschmann, Mechanical Properties of Wood. Wood Handbook-Wood As an Engineering Material, General Technical Report FPL-190, USDA Forest Service, 2010, pp. 1–46.
[61] K.V.P.P. Chandu, Rao E. Venkateswara, Rao A. Srinivasa, B.V. Subrahmanyam, The strength of friction stir welded aluminium alloy 6061, Int. J. Res. Mech. Eng. Technol. 4 (1) (2013) 119–122.
[62] G.B. Hu, et al., Metastructure with piezoelectric element for simultaneous vibration suppression and energy harvesting, J. Vib. Acoust. Transact. ASME 139 (1) (2017).